Phytopathology® • 2021 • 111:703-712 • https://doi.org/10.1094/PHYTO-08-20-0357-R

The Physiological and Biochemical Effects on Napier Grass Plants Following Napier Grass Stunt Phytoplasma Infection

George O. Asudi,[1,2,†] Keziah M. Omenge,[3] Maria K. Paulmann,[1,4] Michael Reichelt,[4] Veit Grabe,[5] Axel Mithöfer,[6] Ralf Oelmüller,[1] and Alexandra C. U. Furch[1]

[1] Department of Plant Physiology, Matthias-Schleiden-Institute for Genetics, Bioinformatics and Molecular Botany, Friedrich-Schiller-University, Dornburger Strasse 159, 07743 Jena, Germany
[2] Department of Biochemistry, Microbiology and Biotechnology, Kenyatta University, P.O. Box 43844, 00100 Nairobi, Kenya
[3] Department of Genetics, Matthias-Schleiden-Institute for Genetics, Bioinformatics and Molecular Botany, Friedrich-Schiller-University, Dornburger Strasse 159, 07743 Jena, Germany
[4] Department of Biochemistry, Max-Planck Institute for Chemical Ecology, Hans-Knöll-Str. 8, 07745 Jena, Germany
[5] Department of Evolutionary Neuroethology, Max Planck Institute for Chemical Ecology, Hans-Knöll-Str. 8, 07745 Jena, Germany
[6] Research Group Plant Defense Physiology, Max-Planck Institute for Chemical Ecology, Hans-Knöll-Str. 8, 07745 Jena, Germany
Accepted for publication 28 September 2020.

ABSTRACT

Napier grass stunt (NGS) phytoplasma, a phloem-limited bacterium, infects Napier grass leading to severe yield losses in East Africa. The infected plants are strongly inhibited in growth and biomass production. In this study, phytoplasma-induced morphological changes of the vascular system and physiological changes were analyzed and compared with uninfected plants. The study showed that the phytoplasmas are more abundant in source leaves and range from 10^3 bacteria/µg total DNA in infected roots to 10^6 in mature Napier grass leaves. Using microscopical, biochemical, and physiological tools, we demonstrated that the ultrastructure of the phloem and sieve elements is severely altered in the infected plants, which results in the reduction of both the mass flow and the translocation of photoassimilates in the infected leaves. The reduced transport rate inhibits the photochemistry of photosystem II in the infected plants, which is accompanied by loss of chloroplastic pigments in response to the phytoplasma infection stress eventually resulting in yellowing of diseased plants. The phytoplasma infection stress also causes imbalances in the levels of defense-related antioxidants, glutathione, ascorbic acid, reactive oxygen species (ROS), and—in particular—hydrogen peroxide. This study shows that the infection of NGS phytoplasma in the phloem of Napier grass has an impact on the primary metabolism and activates a ROS-dependent defense response.

Keywords: bacterial pathogens, etiology, host parasite interactions, Napier grass stunt phytoplasma, pathogen detection, phloem mass flow, photoinhibition, plant immune responses, plant stress and abiotic disorders, H_2O_2

Napier or elephant grass (*Pennisetum purpureum* Schumach) is an essential fodder crop in East Africa. However, its continued production is under severe threat of Napier grass stunt (NGS) disease (Asudi et al. 2015; Kawube et al. 2015). The NGS disease is caused by a phytoplasma, an uncultivable cell wall-less obligate mollicute that originated through degenerate evolution from Gram-positive prokaryotes. Globally, phytoplasmas cause numerous plant diseases of grasses, vegetables, crops, fruits, and ornamental plants resulting in phytosanitary conditions and severe losses of world economies (Asudi et al. 2015; Kawube et al. 2015; Lee et al. 2000). In Napier grass plants, the phytoplasma induces characteristic symptoms such as small leaves, foliar yellowing, proliferation of tillers, and shortened internodes. These symptoms often become apparent after regrowth of the infected plant after animal grazing or several cuttings, which usually lead to the death of the infected plants (Asudi et al. 2015; Jones et al. 2004; Kabirizi et al. 2007; Kawube et al. 2015). Young leaves of infected sugarcane (*Saccharum officinarum*) plants also develop yellow symptoms but are characterized by bright yellow midribs in late stages of the plants' growth. However, in several cereals, including finger millet (*Eleusine coracana*), maize (*Zea mays*), sorghum (*Sorghum bicolor*), pearl millet (*Pennisetum glaucum*), and rice (*Oryza sativa*), the NGS infection occurs without causing visible symptoms (Asudi et al. 2016a). The bacterium is spread from one place to another through the propagation of infected root splits or stem cuttings (Asudi et al. 2015; Koji et al. 2012), from which it is transmitted to phloem sieve elements (SEs) of healthy plants by insect vectors, mainly the leafhopper *Maiestas banda* (Kramer) (Hemiptera: Cicadellidae) (Asudi et al. 2016a, 2019; Obura et al. 2009; Wamalwa et al. 2017).

Because phytoplasmas have not been cultured in vitro, their detection and identification are limited to molecular tools. Besides serological assays (Lee et al. 2000) and including monoclonal antibodies against an immunodominant membrane protein (*imp*) of the phytoplasma (Wambua et al. 2017), various species-specific primers based on the 16S ribosomal gene are used to detect the pathogen in plants and insects (Lee et al. 1998, 2000; Obura et al. 2011; Wamalwa et al. 2017). The 16S rDNA sequence information demonstrates that phytoplasmas belonging to the 16SrXI group or '*Candidatus* Phytoplasma oryzae' are the major cause of the NGS disease in Tanzania, Uganda, and Kenya (Asudi et al. 2016b; Jones et al. 2004; Kawube et al. 2015; Nielsen et al. 2007; Obura et al. 2009).

Despite the enormous economic losses because of NGS phytoplasma, the molecular basis of the host responses to the infection is not well understood. Phytoplasmas reside strictly in the phloem SEs from where they systemically spread to the whole plant through the sieve plate pores (Christensen et al. 2004, 2005; Lee et al. 2000; Musetti et al. 2013, 2016). Consequently, the phloem transport system is impaired—leading to the accumulation of

†Corresponding author: George O. Asudi; gasudii@gmail.com

Funding: Support was provided by Alexander von Humboldt-Stiftung, Germany.

First and second authors contributed equally to this work.

The author(s) declare no conflict of interest.

carbohydrates in the source leaves, reduction in photosynthetic rates, and lack of sugars in sink tissues (Christensen et al. 2004, 2005; Gai 2014; Lepka et al. 1999; Liu et al. 2016). Plants respond to phytoplasma infection by activating their immune system, which includes hormone changes in the infected tissues (Das and Mitra 1998; Dermastia 2019; León et al. 1996; Mardi et al. 2015; Sánchez-Rojo et al. 2010; Zimmermann et al. 2015). However, the phytoplasma developed mechanisms to escape the phytohormone-induced plant defense by suppressing host immunity. For example, an aster yellows phytoplasma strain produces the SAP11 effector, which represses jasmonic acid (JA) biosynthesis in *Arabidopsis* plants (Gai 2014; Sugio et al. 2011). The plant defense response also includes the generation of reactive oxygen species (ROS) such as singlet oxygen, superoxide anions, hydroxyl radicals, and hydrogen peroxide (H_2O_2), as shown for phytoplasma-infected apple (*Malus domestica*), grapevine (*Vitis vinifera*), peach (*Prunus persica*), and apricot (*P. armeniaca*) plants (Gambino et al. 2013; Musetti et al. 2005, 2007). Therefore, the objective of this study was to determine the physiological and biochemical changes that occur in Napier grass plants after NGS-phytoplasma infection. Our data suggest that the reduced growth rate of the NGS-phytoplasma-infected plants is caused by alterations in the phloem morphology and mass flow through the plant organs. These may result in changes in the sink/source relationship and the activation of plant defense responses against the NGS phytoplasma.

MATERIALS AND METHODS

Plant materials. Napier grass (cultivar Ouma-2) cuttings infected with '*Ca*. P. oryzae' strain NGS were obtained from diseased Napier grass plants with yellow to purple streaking and stunted growth at the International Centre of Insect Physiology and Ecology, Mbita Research Station, Kenya (0°25′50′′S, 34°12′27′′E). Cuttings from Napier grass of the (cv. Ouma-2) that were not infected with NGS were also obtained from the same station. The grass cuttings were grown in pots and maintained in a greenhouse under 8 h of darkness and 16 h of light (25°C, 65% relative humidity) for 3 months in Jena, Germany.

Isolation, amplification, and quantification of phytoplasma DNA in Napier grass plants. Genomic DNA was extracted from 0.3 g of fresh leaf samples of Napier grass by the CTAB extraction method, as described in Obura et al. (2009). The concentrations of DNA were determined with a NanoVue Plus Spectrophotometer (GE Healthcare, Chicago, IL) and quality-verified using 1% (wt/vol) agarose gel electrophoresis. The 16S rRNA gene was amplified using the universal primer pair P1/P6 (Deng and Hiruki 1991) in the first-round PCR followed by a second PCR with the primer pair NapF/NapR (Obura 2012). The initial amplification was performed in a 10-µl PCR reaction mixture containing genomic DNA, 10× PCR buffer (Thermo Fisher Scientific, Vilnius, Lithuania), 0.2 mM of dNTPs, 5 units of DreamTaq DNA polymerase (Thermo Fisher Scientific), and 400 µM of each primer (Eurofins Genomics, Germany, Ebersberg, Germany). PCR reactions were carried out in a Proflex PCR machine (Applied Biosystems, Foster City, CA) as follows: 94°C for 3 min; 35 cycles of denaturation at 94°C for 30 s, then annealing at 53°C for 90 s and extension at 72°C for 90 s; and a final elongation step at 72°C for 10 min. DNA amplified in the initial PCR was vortexed gently and 0.6 µl used as a template in a nested PCR with the same conditions except for the annealing temperature at 56°C. Amplicons were visualized by gel electrophoresis in a 1% agarose gel stained with ethidium-bromide using 1× TBE (40 mM of Tris-acetate and 1 mM of EDTA at pH 8.0) as running buffer, and photographed. The presence of the NGS phytoplasma was also confirmed by amplification of the species-specific *imp* gene using the Fimp_NGS_n/Rimp_NGS_n primer pair (Wambua et al. 2017). In all experiments, water controls without DNA (negative controls) and the DNA from the reference NGS phytoplasma strain (as a positive control) were included.

The titer of the NGS phytoplasma was determined for 0.1 g of DNA in a quantitative real time-PCR assay as described by Christensen et al. (2004) with a few modifications. The PCR reactions were carried out in triplicate in a 10-µl PCR mixture with 20 ng of total DNA using DreamTaq (Thermo Fisher Scientific), 0.2 mM of dNTPs, and 200 nM of each forward and reverse primer in a CFX96 Touch Real-Time PCR machine (Bio-Rad Laboratories, Hercules, CA). The fluorogenic probes for phytoplasma and plant DNA were synthesized by Eurofins Genomics, Germany, and labeled according to Christensen et al. (2004) except for the 5′ end of the plant DNA probe, which was labeled with hexachlorofluorescein. The standard equation $y = -3.264x + 41.73$ ($R^2 = 0.9778$) was used to convert the individual cycle threshold (Ct) values into the bacteria/cell based on the extracted DNA (in micrograms; Christensen et al. 2004, 2013).

Bioimaging of phytoplasma infection. Phytoplasmas were visualized in infected Napier grass plant leaves using DNA-specific 4′,6-diamidino-2-phenylindole (DAPI) dye prepared in dimethyl sulfoxide (1 mg/ml). For confocal laser scanning (CLS) microscopy, cross sections of Napier grass leaves were taken using a fresh razor blade and stained with 0.3 µM of DAPI. After 30 min of incubation, DAPI-stained cross sections of Napier grass leaf tissues were imaged using a CLS microscope 880 (Zeiss Microscopy, Jena, Germany) with the 405-nm laser line. Images were taken with a 40× objective (Plan-Apochromat 40×/0.8). Lambda stacks were created using the 32-channel GaAsP detector followed by Linear Unmixing with the software ZEN (Zeiss Microscopy). Z-stacks were taken from specific areas of the sample, and Maximum Intensity Projections were produced with the ZEN software.

Determination of the rate of mass flow and anatomical changes in vascular tissues. The phloem-mobile dye, 5,6 carboxyfluorescein diacetate (5(6)-CFDA; containing 2 mol/liter of KCl, 1 mol/liter of $CaCl_2$, 1 mol/liter of $MgCl_2$, 50 mol/liter of mannitol, and 2.5 mol/liter of MES/NaOH buffer, at pH 5.7) was used to investigate phloem mass flow in healthy and infected Napier grass leaves as described in Musetti et al. (2013). Potted plants were laid vertically, and the leaf tip of each leaf removed using a razor blade. The cut part of the leaf tip was immediately immersed into a freshly prepared 1-µM 5(6)-CFDA solution and incubated for 30 min at room temperature. After incubation in the dye, rates of mass flow were determined by the furthest distance the fluorescent dye had moved from the tip of the leaf by examining thin cross sections made with fresh razor blades which were then mounted on a fluorescent microscope slide (AXIO Imager M2, Zeiss Microscopy).

The physiological state of the vascular tissue was assessed using a microscope with a 40× buffer immersion objective, and the phloem tissue examined at 488 nm. Measurements of the areas of the vascular bundles, phloem, xylem vessels, whole xylem area, and SEs were recorded, and the digital images taken by a color 164 camera (AXIOCAM 503 color, Zeiss Microscopy). The widths and the lengths of every second and third leaf were measured in centimeters with a ruler from one side (tip) of the leaf to the other side (stalk). The rates of mass flow of the phytoplasma-infected and healthy plant leaves were recorded after 30 min of incubation in 5(6)-CFDA solution and expressed as distance (in centimeters) over time (hours). The whole area of the vascular bundle tissue represented the area containing the xylem vessels, phloem, and the SEs measured in μm^2. The numbers of xylem vessels were recorded, and the entire area occupied the xylem vessels, SEs, and the phloem measured in μm^2. The areas of the SEs represented an average of four visible SEs.

Pigment analysis and chlorophyll fluorescence measurements. Chlorophyll and carotenoids were extracted with buffered acetone (containing acetone, water, and ammonia [25% wt/vol] prepared in the ratio 160:39:1) from 100 mg of leaf material under the dark condition for 30 min. The chlorophyll and carotenoids contents were analyzed by a biospectrophotometer (Eppendorf, Hamburg,

Germany) as described by Lichtenthaler (1987). Measurements of chlorophyll fluorescence on detached leaves were performed with a FluorCam7.0 fluorometer (Walz, Effeltrich, Germany) at ambient CO_2 and temperature. Before each analysis, the potted plants were dark-adapted for 30 min. The minimum fluorescence in the dark-adapted state (F_o) was measured for 2 s after dark adaptation followed by a saturating light pulse that lasted 960 ms to induce maximum fluorescence (F_m) in the dark-adapted state. The leaf sample was then exposed to actinic light for 71 s, and the Kautsky effect with a saturating light pulse of 3 s and peak fluorescence (F_p) was recorded. Subsequently, a saturating pulse was applied to reduce transiently the plastoquinone pool during the actinic light exposure to measure the maximum fluorescence during light adaptation (F_m_Ln) at 9 s for F_m_L1, 19 s for F_m_L2, 29 s for F_m_L3, and 49 s for F_m_L4, respectively. The maximum fluorescence at the light-adapted steady state (F_m_Lss) was obtained during the saturating flash (t = 69 s) at the end of actinic light period. The instantaneous maximum fluorescence signals during dark relaxation (F_m_Dn) with saturating pulses at 131 s for F_m_D1, 161 s for F_m_D2, and at 322 s for F_m_D3 were also measured. From the measured fluorescence signals, the variable fluorescence in the dark-adapted state ($F_v = F_m - F_o$), the maximum quantum efficiency of photosystem II (PSII) ($F_v/F_m = [F_m - F_o]/F_m$), instantaneous nonphotochemical quenching (NPQ) during light adaptation ($NPQ\_Ln = [F_m - F_m\_Ln/F_m\_Ln]$) and steady-state nonphotochemical quenching in light ($NPQ\_Lss = [F_m - F_m\_Lss/F_m\_Lss]$) were obtained as described in Cen et al. (2017). Other chlorophyll fluorescence parameters for the evaluation of the photosynthetic efficiency at steady-state conditions included the coefficient of photochemical quenching in steady-state light (qP) and qL, which estimates the fraction of open PSII centers.

Estimation of the ROS and the antioxidants. Total ROS was determined with 10 µM of 2,7-dichlorofluorescein diacetate (Sigma-Aldrich, Steinheim, Germany) as described by Paulmann et al. (2018). Powdered plant leaves (40 mg) were extracted with 500 µl of 10 mM of Tris-HCl buffer (pH 7.2) and the extract diluted 40 times with the same buffer. ROS was measured in triplicates using a black 96-well plate with H_2O_2 as an external standard. Emitted fluorescence was measured for 10 s per well with a Synergy H4 hybrid multimode microplate reader (BioTek Instruments, Winooski, VT) using optimal gain and xenon flash while the fluorophore was excited at wavelengths of 485 nm and the emission recorded at 530 nm. For the glutathione (GSH) and ascorbic acid (AsA) assays, 40 mg of freshly powdered plant tissue was extracted using 500 µl of 5% (wt/vol) meta-phosphoric acid solution and then gently shaken for 5 min at 4°C followed by centrifugation at 15,000 RCF for 15 min and 4°C. The supernatant was transferred into a microcentrifuge tube and stored at –80°C before use. After thawing, the supernatant was diluted 1:10 with water that contained labeled GSH (glutathione-glycine-$^{13}C2$, ^{15}N disodium salt [BIOZOL Diagnostica Vertrieb, Eching, Germany]) as the internal standard. Three microliters of this mixture were injected into an Agilent 1260 HPLC system (Agilent Technologies, Santa Clara, CA). Prepared labeled GSH 1 µg/ml standards were diluted 873 times and used as internal standards. The samples were then mixed with the standards in the ratio of 1:10. The standards for creating the curves were prepared by mixing 40 µl of AsA (0.25 mg/ml) or GSH (0.25 mg/ml) (in meta-phosphoric acid solution) to 2 µl of oxidized glutathione (GSSG) before addition of sterile water to 400 µl. The first standard was prepared by diluting the mixture three times.

The chromatographic separation was achieved at a temperature of 25°C on a Sphinx column (EC 260/4.6 Nucleodur Sphinx RP, 5 µm [Macherey-Nagel, Düren, Germany]) with a mobile phase consisting of different ratios of 0.2% (vol/vol) formic acid (FA; liquid chromatography-mass spectrometry [LC-MS] grade, Thermo Fisher Scientific, Geel, Belgium) and acetonitrile (ACN; LC-MS grade, VWR Chemicals, Radnor, PA). The flow rate was maintained at 1 ml min^{-1} and the ratios changed as follows: 0 to 3.5 min, 98% of 0.2% FA; 3.5 to 5.0 min, 98 to 0% of 0.2% FA; 5.0 to 8.0 min, 100% ACN; and 8.0 to 12.0 min, 98% of 0.2% FA. In the API 5000 tandem mass spectrometer (Applied Biosystems, Foster City, CA) the analyte parent ion → product ion fragmentation was monitored via multiple reaction monitoring (MRM) with the MRMs expected as listed in the following: m/z 306.2→143 (collision energy [CE] –28 V) for GSH; m/z 611.2→306 (CE –34 V) for GSSG; m/z 309.2→143 (CE –28 V) for the labeled GSH*; m/z 617.2→309 (CE –34 V) for the oxidized labeled GSSG*; m/z 175.2→115 (CE] –18 V) for AsA; and m/z 173.2→113 (CE –14 V) for the oxidized AsA.

The declustering potential (DP) was maintained at –60 V for all measured analytes, the ion spray voltage was kept at –4,500 eV, and the turbo gas temperature was set to 700°C. Nebulizing and heating gas values were set to 70 pounds of force per square inch (psi), the curtain gas to 35 psi, and the collision gas to 4 psi. The response factors were determined using an averaged external standard curve performed at each measurement day. GSH* and GSH (Sigma-Aldrich) were assumed to have the same response factor whereas the response factor for GSSG (from the Amplite Fluorimetric Glutathione GSH/GSSG Ratio Assay Kit [AAT Bioquest, Sunnyvale, CA]) and AsA (Carl Roth, Karlsruhe, Germany) were 0.19 and 1.18, respectively. The data were analyzed with the software Analyst 1.6 (Applied Biosystems).

Quantification of phytohormones in phytoplasma-infected and uninfected plants. For phytohormone analyses, two leaf samples were harvested from each plant and immediately frozen in liquid nitrogen and stored at –20°C. The leaf samples (250 mg) were homogenized using a Geno/Grinder (Spex CertiPrep, Stanmore, UK) at 1.100 rpm for 1 min and extracted in 1.5 ml of methanol containing 60 ng of D_4-salicylic acid (D_4-SA [Santa Cruz Biotechnology, Dallas, TX]), 60 ng of D_6-jasmonic acid (D_6-JA [HPC Standards, Cunnersdorf, Germany]), 60 ng of D_6-abscisic acid (D_6-ABA [Santa Cruz Biotechnology]), 12 ng of D_6-JA-Ile (HPC Standards, Cunnersdorf, Germany), and 10 ng of D_5-indolacetic acid (D_5-IAA [OlChemIm, Olomouc, Czech Republic]) as internal standards. Samples were agitated on a horizontal shaker at room temperature for 10 min. The homogenate was mixed for 30 min and centrifuged at 13,000 rpm for 20 min at 4°C, and the supernatant was collected. The homogenate was re-extracted with 500 µl of methanol, then mixed and centrifuged before evaporation (speed-vacuum) under reduced pressure at 30°C. The final methanolic crude extract was redissolved in 500 µl of methanol. Phytohormone analysis was performed by LC-MS/MS as described by Heyer et al. (2018) on an Agilent 1260 series HPLC system (Agilent Technologies) with a modification that included the use of a tandem mass spectrometer QTRAP 6500 (SCIEX, Darmstadt, Germany). Indole-acetic acid was quantified using the same LC-MS/MS system with the same chromatographic conditions but using positive mode ionization with an ion spray voltage at 5,500 eV. MRM was used to monitor analyte parent ion into product ion fragmentations as follows: m/z 176→130 (CE 19 V; DP 31 V) for IAA and m/z 181→133 + m/z 181→134 + m/z 181 →135 (CE 19 V; DP 31 V) for D_5-IAA.

Data analysis. The data of the phytoplasma titer, areas of vascular tissues, phloem mass flow rate, levels of H_2O_2, antioxidants, and rates of photosynthesis were subjected to descriptive statistics and expressed as mean ± standard error of mean. Independent t test using the Statistical Package for Social Sciences (SPSS) version 18 (SPSS Inc., Chicago, IL) was carried out to obtain statistical significance differences between means of different treatments in phytoplasma-infected and uninfected plants. The value $P \leq 0.05$ was considered significant. Two standard curves were made—one for phytoplasma quantification and the other for quantification of plant DNA. The DNA for the phytoplasma standard curve was obtained from one phytoplasma-infected Napier grass leaf after amplification with the primer pair P1/P6 and NapF/NapR (Deng and Hiruki 1991; Obura 2012). For the standard curves, the obtained amplicon was diluted 10-fold in a series (10° to

10^{-6}). The number of phytoplasma copies was calculated based on molecular weight using the formula:

$$\text{number of copies} = \left(\frac{\text{amount of DNA in nanograms} \times \text{Avogadro's number}}{\text{length in base pairs} \times 1 \times 10^{9} \times 650}\right)$$

where Avogadro's number = 6.023×10^{23}. The quantities of phytoplasma in source leaves, second leaves, and the roots were subjected to analysis of variance using the software SPSS version 18 (SPSS Inc.).

RESULTS

Detection and quantification of NGS phytoplasma in the different tissues. Phytoplasma-infected Napier grass plants were characterized by foliar yellowing, small leaves, proliferation of tillers, and shortening of internodes with severely stunted clumps (Fig. 1B). A 778-bp DNA fragment was amplified in the diseased plants using the NapF/NapR primer pair targeting the phytoplasma 16S rRNA gene (Fig. 1C). Further, the presence of phytoplasma was confirmed in the phytoplasma-infected Napier grass leaves with the primer pair targeting a 500-bp fragment of the *imp* gene (Fig. 1D). In contrast, no product was amplified from the DNA of the leaves of healthy plants (Fig. 1A). The NGS-phytoplasma titer was quantified in the first and second leaf and the roots. Based on the *Ct* values and standard equation (see "Materials and Methods"), the number of bacteria/microgram total DNA was estimated (Table 1). The NGS-phytoplasma were most abundant in the oldest first leaf and lower in the second leaf and the roots (Table 1), although the titers were not significantly different: $F_{(2,6)} = 1.676$, $P = 0.264$.

Localization of phytoplasma cells in Napier grass leaves. Cross- and longitudinal hand sections of infected and healthy Napier grass leaves were stained using the DNA-specific dye DAPI to detect the phytoplasma colonization and analyzed using a CLS microscope. The study showed the formation of dense masses of phytoplasmas in the sieve tubes of NGS phytoplasma-infected plants (Fig. 2B and D; which filled the cell lumen) compared with healthy plants where no fluorescence was detected (Fig. 2A and C). The fluorescent dots and aggregated spots accumulated predominantly on the membranes of the sieve plates in the longitudinal sections of phytoplasma-infected leaves (Fig. 2F) while the healthy control sections showed no DAPI-specific fluorescence on the membrane of the sieve tubes (Fig. 2E).

The NGS-phytoplasma infection impacts on the leaf and vascular morphology of Napier grass leaves. Figure 1 and previous studies showed that NGS-phytoplasma-infected Napier grass is impaired in growth and biomass production (Asudi et al. 2015, 2016a, b; Jones et al. 2004; Kabirizi et al. 2007; Kawube et al. 2015; Nielsen et al. 2007). In this study, we found that the

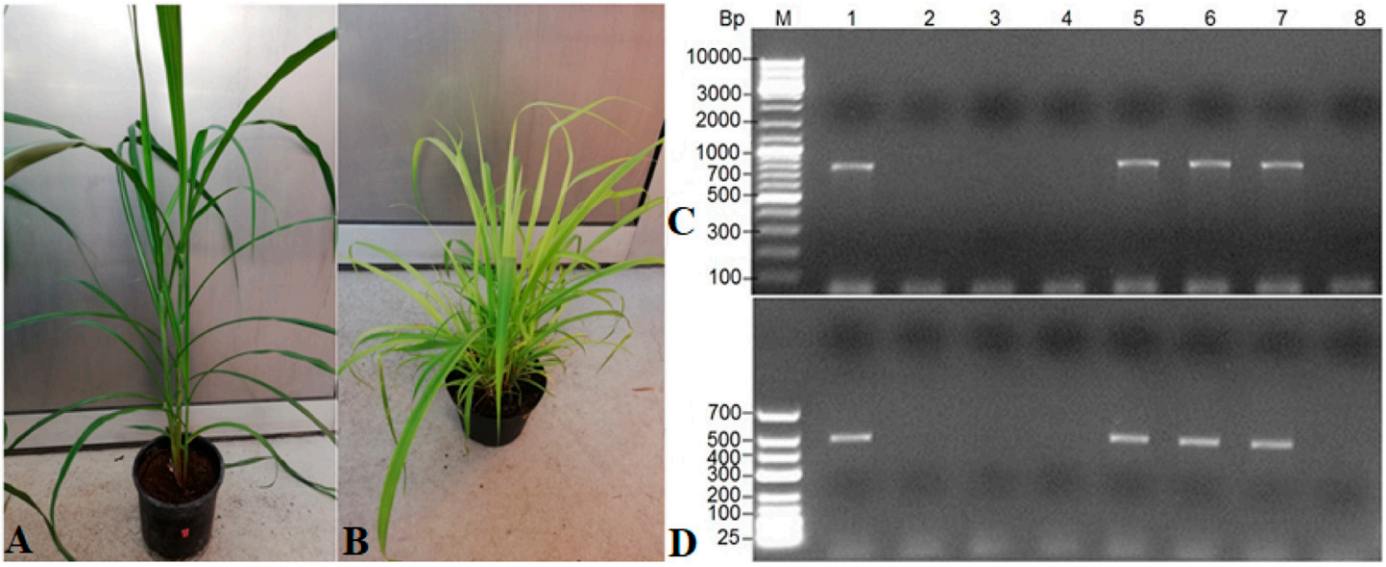

Fig. 1. Picture showing **A,** healthy Napier grass plant and **B,** severely stunted, bushy Napier grass with foliar yellowing and reduced biomass of phytoplasma-infected plant. **C,** Electropherogram of 16SrDNA fragment amplimers amplified with P1/P6 followed by NapF/NapR primers. **D,** *imp* gene-amplimers using Fimp_NGS_n/Rimp_NGS_n primer pair. Analyzed samples are the same in A and B, except for the size marker (lane M), which was 1 kb of DNA marker GeneRuler mix (Thermo Fisher Scientific) in A and GeneRuler Low Range DNA Ladder (Thermo Fisher Scientific) in B. Lane 1, reference strain '*Candidatus* Phytoplasma oryzae' Mbita1; lanes 2, 3, and 4, uninfected plants; lanes 5, 6, and 7, phytoplasma-infected Napier grass plants; and lane 8, negative control (water).

TABLE 1. Infection level in individual Napier grass plants analyzed with TaqMan assay

Tissue	Plant	C_T, 16S (phytoplasma)	C_T, 18S (plant)	Normalized mean quantity (cells/µg of total DNA extracted)
Leaf 2	Plant 1	24.40 ± 0.20	14.48 ± 0.26	6.53×10^4
Leaf 2	Plant 2	23.57 ± 0.20	14.35 ± 0.34	1.50×10^5
Leaf 2	Plant 3	24.65 ± 0.07	15.03 ± 0.53	8.11×10^4
Leaf 1	Plant 1	21.62 ± 0.07	14.39 ± 0.33	6.61×10^5
Leaf 1	Plant 2	19.50 ± 0.27	11.65 ± 9.12	3.01×10^6
Leaf 1	Plant 3	23.21 ± 0.40	13.89 ± 0.29	1.22×10^5
Roots	Plant 1	24.22 ± 0.17	19.53 ± 0.58	8.65×10^3
Roots	Plant 2	22.75 ± 0.26	16.63 ± 0.77	8.33×10^4
Roots	Plant 3	20.28 ± 0.23	14.95 ± 0.30	2.80×10^5

NGS-phytoplasma significantly reduces the leaf sizes (length and width) and negatively affects the size of the mid-vascular tissues in Napier grass (Table 2). Because phytoplasmas are restricted to the phloem sieve tubes (Musetti et al. 2013, 2016), the specific impact of the NGS-phytoplasma infection on the vascular morphology was investigated by analyzing the areas of vascular bundle, xylem, phloem, and SEs (Fig. 3A). The areas of the whole vascular bundle, phloem, entire xylem vessels, xylem vessels (Fig. 3B), and SEs (Fig. 3C) were significantly larger in healthy leaves compared with those found in diseased leaves.

The NGS-phytoplasma infection impairs rate of phloem mass flow in Napier grass. Because the phloem areas were considerably reduced in the infected leaves, we measured the phloem mass flow. After 30 min, the phloem-mobile fluorescence dye 5(6)-CFDA moved 30.31% significantly faster in the phloem tissues of healthy compared with NGS phytoplasma-infected plant leaves. This indicates that the phytoplasma impairs the transport through the phloem sieve tubes (Fig. 4).

The NGS-phytoplasma infection inhibits photosynthesis in Napier grass. Because lower phloem transport rates influence photosynthesis (Christensen et al. 2004; Gai 2014; Lepka et al. 1999; Liu et al. 2016), we determined the effects of phytoplasma infection on PSII photochemistry in Napier grass leaves. The F_v/F_m values of phytoplasma-infected plants were significantly lower than those of uninfected leaves. This indicates that the photochemistry at PSII in the NGS phytoplasma-infected leaves is reduced because of competition with thermal decay processes in the light (Oxborough and Baker 1997). Consistent with this result, the *NPQ* value, a rate constant for heat loss from PSII, increased in NGS phytoplasma-infected leaves compared with the value in healthy plants. The slightly but significantly reduced F_v/F_m value for the maximum quantum yield of photosynthesis after dark-adaptation (Björkman and Demmig 1987) confirms that the infected plants are stressed. The proportion of open PSII reaction centers was also reduced in infected leaves, as indicated by the *qP* and *qL* values. Taken together, changes in chlorophyll fluorescence parameters show that the NGS-phytoplasma infection impairs PSII photochemistry in Napier grass leaves. Furthermore, F_v/F_o was significantly decreased in unhealthy leaves (Fig. 5A), indicating reduced photosynthetic rates.

Further analysis of chlorophyll fluorescence parameters was obtained during the fluorescence quenching process (Fig. 5). The F_v/F_o (Fig. 5B) and F_v/F_m (Fig. 5C) values were consistently lower in infected leaves at different states. The results also showed consistent decrease in instantaneous NPQ at several states in response to the NGS phytoplasma infection in Napier grass (Fig. 5D).

TABLE 2. Effect of NGS phytoplasma infection on growth parameters of Napier grass

Variable (cm)	Healthy plants	Diseased plants	*t*	*df*	*P*
Leaf length	67.69 ± 2.17	48.00 ± 2.18	6.403	14	0.00001
Leaf width	1.53 ± 0.11	1.13 ± 0.07	3.008	14	0.00939
Mid-vascular tissue	0.06 ± 0.003	0.05 ± 0.005	3.026	14	0.00907

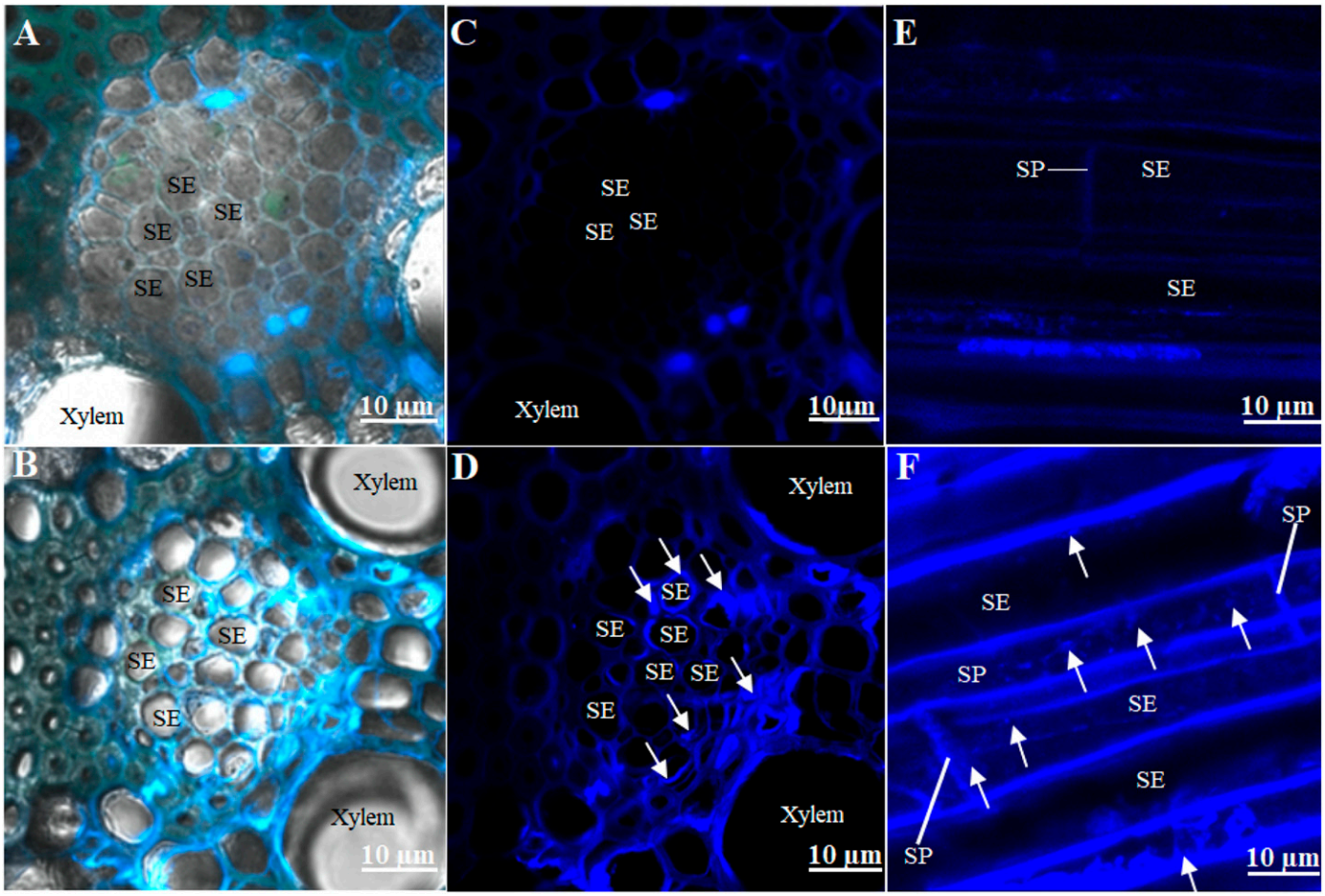

Fig. 2. A, C, and E, Confocal laser scanning micrographs of healthy and **B, D, and F,** NGS-phytoplasma–infected Napier grass leaf tissues. **A and C,** The cross sections of mid-rib phloem tissues of healthy and **B and D,** phytoplasma-infected Napier grass were stained with 4,6-diamidino-2-phenylindole (DAPI) dye, which (arrows; phytoplasma) mainly aggregates at the sieve plates (SP). **F,** The DAPI-stained longitudinal sections show the phytoplasma staining along with the whole sieve element and not just the aggregate at the sieve plates. **A, C, and E,** Phloem in healthy plants remains unlabeled apart from the stained nuclei.

To investigate whether the alterations in the photosynthetic activities were consistent with chlorophyll fluorescence parameters, further analysis for the total chlorophyll and carotenoid contents in leaves of NGS phytoplasma-infected and uninfected Napier grass plants was performed. The chlorophylls *a* and *b*, as well as carotenoid contents, were significantly reduced in the infected leaves (Fig. 6A). The ratios between carotenoids and chlorophylls indicated that there were significant and considerably more carotenoids per chlorophylls molecule in infected leaves than in healthy leaves. Furthermore, the higher chlorophyll *a*/*b* (Fig. 6B) and carotenoid/chlorophyll ratios (Fig. 6C) indicate that the NGS phytoplasma-infected plants suffered under light stress.

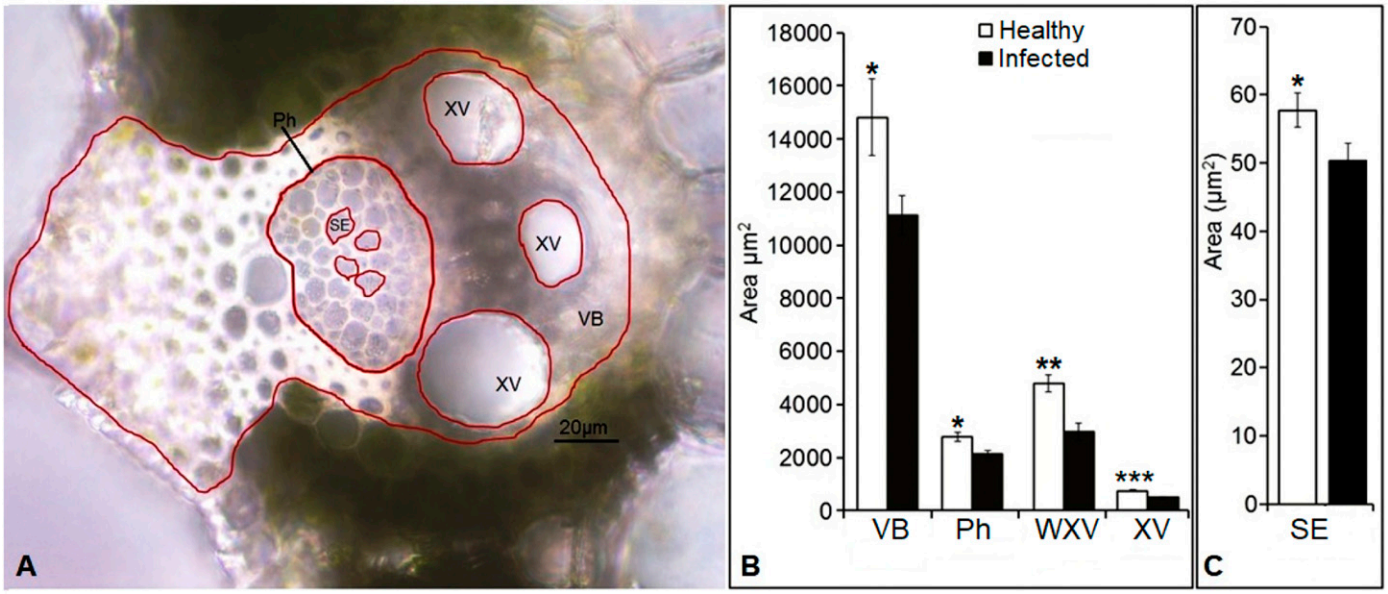

Fig. 3. Analysis of the vascular tissue morphology of healthy and phytoplasma-infected Napier grass plants. **A**, The light microscopic image shows an example of a mid-rib cross section of a healthy Napier grass leaf, indicating the measured areas of vascular bundles (VB), xylem vessels (XV), and phloem tissue (Ph), and the sieve elements (SE) (circled in red color). Scale bar = 20 µm. **B and C,** Graphs show the areas of the whole VB, Ph, areas occupied by all the whole xylem vessels (WXV), XV, and SEs of healthy and infected leaves. The data were expressed as mean ± standard error. Asterisk indicates a statistically significant difference between the infected Napier and the healthy controls (*$P < 0.05$; **$P < 0.01$; ***$P < 0.001$).

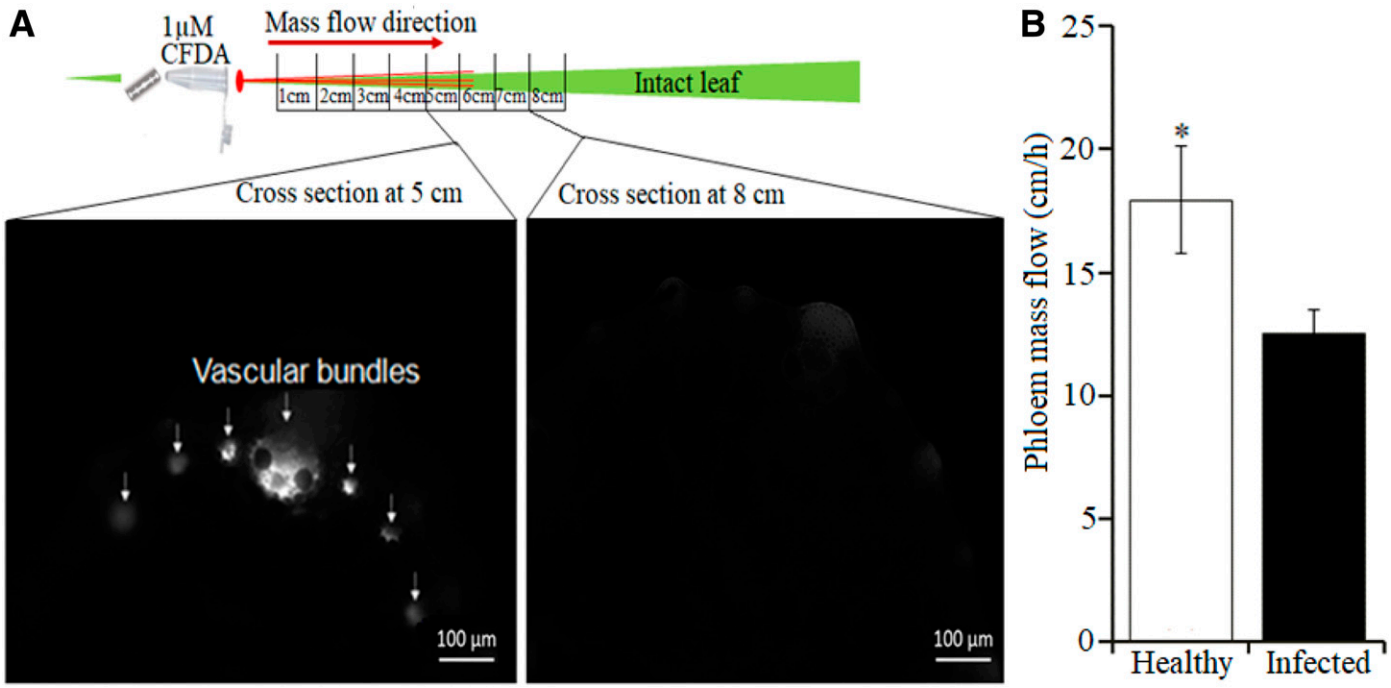

Fig. 4. Analysis of the translocation in phloem sieve elements of healthy and phytoplasma-infected Napier grass plants. **A,** Schematic drawing: The nonfluorescent ester 5,6 carboxyfluorescein diacetate (5(6)-CFDA, membrane-permeable) was continuously applied to the cropped leaf tip and diffused into the sieve elements, where it was cleaved by esterases to form the polar (membrane-impermeable) fluorescent compound carboxyfluorescein (CF). Phloem transport of CF was observed by fluorescence microscopy at cross sections (vertical lines). Carboxyfluorescein was transported by mass flow through sieve tubes until a certain distance after which no CF fluorescence was detected. **B,** The rate of phloem mass flow of healthy and phytoplasma-infected leaves. The results are expressed as the mean ± standard error. Asterisk indicates statistically significant difference between the infected Napier and the healthy control leaves (*$P < 0.05$).

The NGS phytoplasma infection promotes H_2O_2 and reduces GSH and AsA accumulation. In addition to affecting the phloem transport and photosynthesis, ROS may be induced by plants in response to phytoplasma infection stress (Gambino et al. 2013; Musetti et al. 2005, 2007). We measured ROS by approximating the amount of H_2O_2 and determined content changes in GSH and AsA in healthy and infected leaves. NGS phytoplasma-infected leaves accumulated significantly higher amounts of H_2O_2 than healthy plants (Fig. 7A), while the total amount of glutathione was drastically reduced (Fig. 7B). The NGS-phytoplasma also induced GSSG concentration changes in infected plant leaves with significant decline in its contents (Fig. 7B). To ascertain the extent of oxidative stress on the redox state of glutathione, we examined the GSH:GSSG ratio. NGS-phytoplasma infection had small but no significant effect on the GSH:GSSG redox ratio (Fig. 7C). The ascorbate level varied in the investigated healthy leaves but was not always at the detection limit in the infected plants. In contrast, the oxidized dehydroascorbic acid was always detectable and slightly (but not significantly) reduced in the leaves of infected plants (Fig. 7B).

The NGS phytoplasma infection affects the levels of phytohormones. To investigate whether phytohormones are involved in the response of Napier grass to NGS-phytoplasma infection, the contents of ABA, salicylic acid (SA), indole-3-acetic acid (IAA), and JA and four of its derivatives in the infected and healthy leaves were measured. The infected plants accumulated significantly higher amount of *cis*-12-oxophytodienoic acid (cis-OPDA) and low quantities of OH-JA (Fig. 8A). We did not observe significant differences in the contents of ABA, IAA, JA, and sum-JA-Ile (Fig. 8A), OH-JA-Ile and COOH-JA-Ile (Fig. 8B), and SA (Fig. 8C) between phytoplasma-infected and the control plant leaves. However, the concentrations of ABA, IAA, JA (Fig. 8A), and COOH-JA-lle (Fig. 8B) were slightly increased in the phytoplasma-infected plant leaves than in healthy controls, while the concentrations of sum-JA-lle (Fig. 8A), OH-JA-lle (Fig. 8B), and SA (Fig. 8C) were decreased in the infected plant leaves.

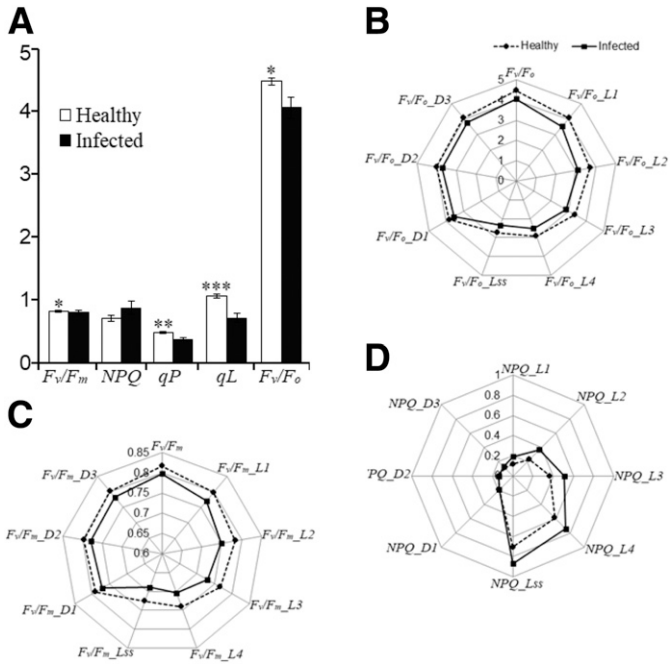

Fig. 5. A, Changes of chlorophyll fluorescence parameters in healthy and NGS-phytoplasma–infected Napier grass. F_v/F_m is the maximum quantum efficiency of photosystem II (PSII) in the dark-adapted state; *NPQ*, the non-photochemical quenching of maximum fluorescence in steady-state light; *qP*, photochemical quenching in steady-state light; *qL*, an estimate of the fraction of open PSII centers; and F_v/F_o, the maximum quantum yield of PSII photochemistry. Asterisk indicates a statistically significant difference between the phytoplasma-infected Napier and the healthy control (*$P < 0.05$; **$P < 0.01$; ***$P < 0.001$). Spider plots of some selected fluorescence parameters including **B,** F_v/F_o; **C,** F_v/F_m; and **D,** NPQ at different states of healthy and NGS phytoplasma-infected Napier grass leaves measured during the fluorescence quenching process. The *Ln* (*L1*, *L2*, *L3*, and *L4*) represents fluorescence (F_v/F_o, F_v/F_m, and NPQ) during light adaptation at 9, 19, 29, and 49 s, respectively; *Lss*, the maximum fluorescence at the light-adapted steady state obtained during the saturating flash ($t = 69$ s) at the end of actinic light period. *Dn* (*D1*, *D2*, *D3*, and *D4*) represents the instantaneous fluorescence signals for F_v/F_o, F_v/F_m, and NPQ during dark relaxation with saturating pulses at 131, 161, and at 322 s, respectively.

DISCUSSION

The study showed that NGS-phytoplasma infection in Napier grass plants causes phloem dysfunction, which probably leads to altered photosynthesis rates in the leaves because of the restriction of the removal of the photoassimilates. The phloem tissue in healthy Napier grass leaves also contained significantly larger SEs compared with those found in NGS phytoplasma-infected plants. This indicates that phytoplasmas damaged the sieve tube functions and reduced the long-distance transport of photoassimilates (Kehr 2006), causing accumulation of carbohydrates in large quantities in mature leaves from the sealing of the SEs (Christensen et al. 2004, 2005; Lepka et al. 1999; Musetti et al. 2013, 2016). In addition, Callose deposition may cause additional constrictions of the sieve tube elements as observed in *Vicia faba* sieve tubes infected by Stolbur phytoplasma. This may affect the intercellular transport of photoassimilates through the sieve pores in phloem (Musetti et al. 2013).

Sealing of SEs in NGS phytoplasma-infected plants can also occur as a general response to pathogen colonization by the plant immune systems to prevent the spread of the pathogen, leading to the release of phytoplasma effectors, and elicitors and redirecting nutrient flows in plants. The reduced phloem mass flow in the infected leaves is also caused by their reduced sizes, which increase the resistance in the phloem mass flow. Moreover, the size of the xylem tissues in the infected leaves was reduced, probably because of the functional association between xylem and phloem (Kehr 2006; Will and van Bel 2006). The proportional decrease of the xylem and phloem tissue areas is consistent with the smaller leaf size.

Phytoplasmas were detected by bioimaging with DAPI staining and PCR (Arismendi et al. 2010; Christensen et al. 2004; Lee et al. 2000; Musetti et al. 2013, 2016). The bioimaging with DAPI staining showed the formation of dense masses of phytoplasmas in the sieve tubes of infected leaf tissues. The DNA in the mature SEs

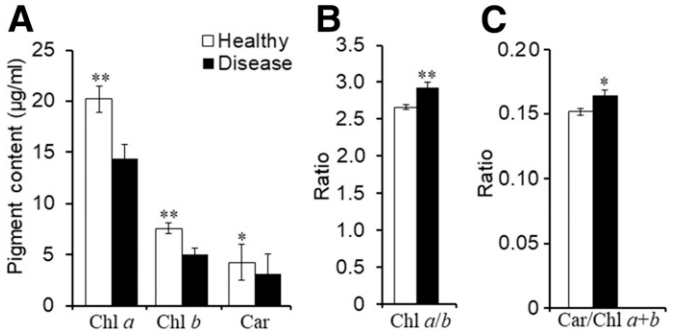

Fig. 6. Changes of pigment contents in phytoplasma-infected and uninfected Napier grass leaves. **A,** *Chl a*, chlorophyll *a*; *Chl b*, chlorophyll *b*; *Chl a+b*, total chlorophyll; and *Car*, carotenoids. **B,** Ratios of *Chl a* to *Chl b* and **C,** carotenoids to the total chlorophyll (*Car/Chl*). Asterisks indicate a statistically significant difference between the phytoplasma-infected Napier and the healthy control (*$P < 0.05$; **$P < 0.01$).

belongs to the phytoplasmas because mature SEs lack nuclei. Furthermore, because the SE cells contain reduced cytoplasm to reduce resistance during photoassimilate transports, the spread and multiplication of phytoplasmas is promoted in diseased plants (Christensen et al. 2005). The PCR analyses showed that the phytoplasma titer was higher in the older developed leaves, which was also found in other phytoplasma-infected plants (Christensen et al. 2004; Wambua et al. 2017). This might be caused by variations in phytoplasma transmissions through insect feeding, or the result of faster propagation in older tissues.

'*Ca.* Phytoplasma' strains affect photosynthetic activities because of inhibited phloem transport and accumulation of the photosynthates in the chloroplasts (Christensen et al. 2004, 2005; Gai 2014; Lepka et al. 1999; Liu et al. 2016). Our study demonstrated a significant reduction in F_v/F_m and pigment composition in infected plants, which indicates lower quantum yields of PSII photochemistry caused by the infection stress (Adhikari et al. 2019; Liu et al. 2016). The decreased F_v/F_m value also reflects damage to PSII reaction centers of the D1 protein (Jiao and Ji 2001), and the lower F_v/F_o value—a measure of the number and size of active photosynthetic reaction centers (Dan et al. 2000; Cen et al. 2017)—might be caused by the slower removal of the photoassimilates from the source leaves. Our findings corroborate those for other phytoplasma-infected plants that have shown deteriorated photosynthesis (Bertamini et al. 2002a, 2002b; León et al. 1996; Liu et al. 2016; Tan and Whitlow 2001).

These conditions promote the formation of triplet chlorophyll under high light intensities, which reacts with oxygen to produce highly damaging singlet oxygen or superoxide anion, and ultimately H_2O_2. The dissipation of this excess excitation energy causes loss of chloroplastic pigments and yellowing of the diseased leaves, often observed for plants infected with phytoplasma (Bertamini et al. 2002a, 2002b; León et al. 1996; Liu et al. 2016; Tan and Whitlow 2001). The small increase in NPQ in infected leaves demonstrates that thermal dissipation of excess excitation energy was insufficient to prevent the photodamage. In addition, the lower *qL* and *qP* values in the infected leaves indicate a change in the balance between excitation rate and electron transfer rate with more reduced PSII reaction centers (Murchie and Lawson 2013). Finally, we found a consistent decrease in the F_v/F_m and F_v/F_o and increase in *NPQ* values, indicating dysfunctions in the electron flow during the dark to light transition (Govindjee 1995). Whether the increase in *NPQ* is a direct effect of the bacterium on PSII because of the irreversible damage, as described for '*Ca.* Liberibacter'-infected citrus (Cen et al. 2017), remains to be determined. The higher carotenoid/chlorophyll ratio also shows that the infected plants activate their ROS scavenging systems. Besides the xanthophyll cycle, carotenoid serves as nonenzymatic scavengers of singlet oxygen (Efeoğlu et al. 2009; Jung et al. 2000). Similar results were found in bois noir-infected grapevines and AY-WB disease-infected lime (*Tilia*) plants (Bertamini et al. 2002a; Zafari et al. 2012).

ROS, especially H_2O_2, are also induced in response to the phytoplasma infection itself, which causes changes in the redox balance and substantial deregulation of the cellular homeostasis. Accumulation of H_2O_2 has also been routinely recorded in phytoplasma-infected plants and is considered one of the most characteristic signs of plant–phytoplasma interactions. For example, H_2O_2 accumulated in mulberry (*Moraceae*) plants infected with the yellow dwarf disease (Gai 2014) and in grapevine, peach, apple, and apricot trees that had spontaneously recovered from phytoplasma infections (Gambino et al. 2013; Musetti et al. 2005, 2007). Plants respond to H_2O_2 production by maintaining a high GSH:GSSG redox ratio. However, because we observed a lower reduced/oxidized glutathione (GSH:GSSG) ratio in infected leaves when compared with the uninfected controls, the ROS scavenging potential of glutathione might be overloaded in the infected leaves. Because more ascorbate was oxidized to DHA, this antioxidant system might be more important to remove excess H_2O_2 accumulation in infected leaves. Furthermore, ascorbate also regulates the redox state of photosynthetic electron carriers through ascorbate peroxidase, and other enzymes via the Mehler reaction (Foyer and Allen 2003; Smirnoff and Wheeler 2000), and its diminutive amounts detected in infected leaves supports the reduced rate of photosynthesis in unhealthy plants.

Many studies have implicated the role of phytohormones in the pathogenicity of phytoplasma, indicating that phytoplasma infection may cause hormonal imbalances in infected plants (Das and Mitra 1998; Dermastia 2019; Gai 2014; León et al. 1996). However, this study showed that most of the phytohormones measured did not show any significant differences between phytoplasma-infected and healthy plants. Generally, the amounts of ABA, IAA, and JA increased while SA declined in unhealthy than in healthy plants. In addition, the increase in *cis*-OPDA and decline in OH-JA suggest perturbations of the JA defense signaling system. Association of phytoplasma infection with reduced or increased levels of JA biosynthesis in young or old leaves of AY-WB phytoplasma-infected Arabidopsis, respectively, have been reported (Sugio et al. 2011). Paolacci et al. (2017) also showed the up-regulation of most

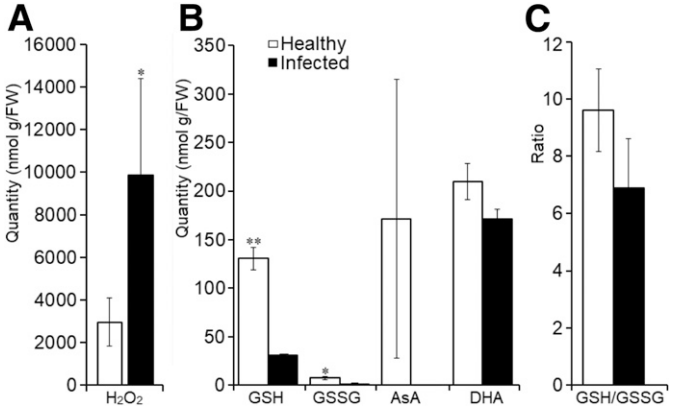

Fig. 7. Distribution of reactive oxygen species (ROS) and nonenzymatic antioxidants in healthy and phytoplasma-infected Napier grass plants. **A,** Quantities of hydrogen peroxide (H_2O_2). **B,** Quantities of nonenzymatic antioxidants in healthy compared with infected plants. GSH, reduced glutathione; GSSG, oxidized glutathione; AsA, ascorbate; and DHA, dehydroascorbic acid. **C,** Ratios of GSH to GSSG. Asterisks indicate a statistically significant difference between the phytoplasma-infected Napier and the healthy control (*$P < 0.05$; **$P < 0.01$).

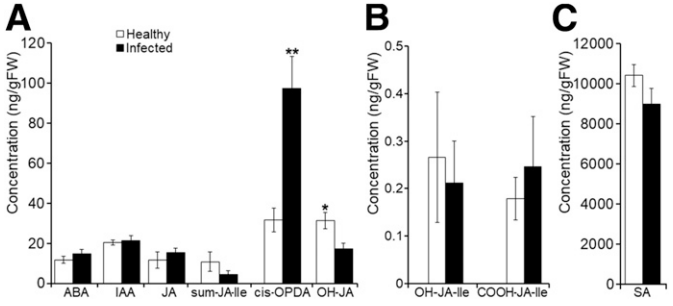

Fig. 8. Concentrations of different phytohormones in response to NGS phytoplasma infection in infected and healthy Napier grass plants. **A,** Concentrations of ABA, abscisic acid; IAA, indole-3-acetic acid; JA, jasmonic acid; sum-JA-Ile, sum (+)-7-*iso*-jasmonoyl-L-isoleucine; cis-OPDA, *cis*-12-oxophytodienoic acid; and OH-JA, 12-hydroxy-JA. **B,** Concentrations of OH-JA-Ile, 12-hydroxy-JA-Ile, COOH-JA-Ile, and 12-carboxy-JA-Ile. **C,** Concentration of SA, salicylic acid. Asterisk indicates a statistically significant difference between the infected Napier and the healthy control (*$P < 0.05$; **$P < 0.01$).

jasmonate biosynthetic genes in the grapevine leaves infected with '*Ca. Phenacoccus solani*' as compared with uninfected plants. This could be true, considering our plants were three months old. This study may also indicate phytohormone changes occur early during disease progression in NGS phytoplasma-infected plants, which was not investigated in this study.

In conclusion, infection of Napier grass by NGS phytoplasma restricts phloem transport from the source to sink tissues. This results in lower photosynthesis rates in the source tissue and higher ROS levels. The plant responds to it by activating its ROS scavenging system.

LITERATURE CITED

Adhikari, N. D., Simko, I., and Mou, B. 2019. Phenomic and physiological analysis of salinity effects on lettuce. Sensors (Basel) 19:4814.

Arismendi, A., Andrade, S., Riegel, S., and Carrillo, L. 2010. Presence of a phytoplasma associated with witches'-broom disease in *Ugni molinae* Turcz. and *Gaultheria phillyreifolia* (Pers.) Sleumer determined by DAPI, PCR and DNA sequencing. Chil. J. Agric. Res. 70:26-33.

Asudi, G. O., Muyekho, F. N., Midega, C. A. O., and Khan, Z. R. 2019. Integrated management of Napier grass stunt disease in East Africa. Pages105-123 in: Sustainable Management of Phytoplasma Diseases in Crops Grown in the Tropical Belt. Sustainability in Plant and Crop Protection, vol. 12, C. Olivier, T. Dumonceaux, and E. Pérez-López, eds. Springer, Cham, Switzerland. https://link.springer.com/chapter/10.1007/978-3-030-29650-6_5

Asudi, G. O., van den Berg, J., Midega, C. A. O., Pickett, J. A., and Khan, Z. R. 2016a. The significance of Napier grass stunt phytoplasma and its transmission to cereals and sugarcane. J. Phytopathol. 164:378-385.

Asudi, G. O., van den Berg, J., Midega, C. A. O., Pittchar, J., Pickett, J. A., and Khan, Z. R. 2015. Napier grass stunt disease in East Africa: Farmers' perspectives on disease management. Crop Prot. 71:116-124.

Asudi, G. O., van den Berg, J., Midega, C. A. O., Schneider, B., Seemüller, E., Pickett, J. A., and Khan, Z. R. 2016b. Detection, identification, and significance of phytoplasmas in wild grasses in East Africa. Plant Dis. 100: 108-115.

Bertamini, M., Grando, M. S., Muthuchelian, K., and Nedunchezhian, N. 2002a. Effect of phytoplasmal infection on photosystem II efficiency and thylakoid membrane protein changes in field grown apple (*Malus pumila*) leaves. Physiol. Mol. Plant Pathol. 61:349-356.

Bertamini, M., Nedunchezhian, N., Tomasi, F., and Grando, M. S. 2002b. Phytoplasma [Stolbur–subgroup (Bois Noir-BN)] infection inhibits photosynthetic pigments, ribulose-1,5-bisphosphate carboxylase and photosynthetic activities in field grown grapevine (*Vitis vinifera* L. cv. Chardonnay) leaves. Physiol. Mol. Plant Pathol. 61:357-366.

Björkman, O., and Demmig, B. 1987. Photon yield of O_2 evolution and chlorophyll fluorescence characteristics at 77 K among vascular plants of diverse origins. Planta 170:489-504.

Cen, H., Weng, H., Yao, J., He, M., Lv, J., Hua, S., Li, H., and He, Y. 2017. Chlorophyll fluorescence imaging uncovers photosynthetic fingerprint of citrus Huanglongbing. Front. Plant Sci. 8:1509.

Christensen, N. M., Axelsen, K. B., Nicolaisen, M., and Schulz, A. 2005. Phytoplasmas and their interactions with hosts. Trends Plant Sci. 10:526-535.

Christensen, N. M., Nicolaisen, M., Hansen, M., and Schulz, A. 2004. Distribution of phytoplasmas in infected plants as revealed by real-time PCR and bioimaging. Mol. Plant-Microbe Interact. 17:1175-1184.

Christensen, N. M., Nyskjold, H., and Nicolaisen, M. 2013. Real-time PCR for universal phytoplasma detection and quantification. Pages 245-252 in: Phytoplasma: Methods and Protocols. M. Dickinson and J. Hodgetts, eds. Springer, New York.

Dan, T. V., Krishnaraj, S., and Saxena, P. K. 2000. Metal tolerance of scented geranium (*Pelargonium* sp. 'Frensham'): Effects of cadmium and nickel on chlorophyll fluorescence kinetics. Int. J. Phytoremediation 2:91-104.

Das, A. K., and Mitra, D. K. 1998. Hormonal imbalance in brinjal tissues infected with little leaf phytoplasma. Indian Phytopathol. 51:17-20.

Deng, S., and Hiruki, C. 1991. Amplification of 16S rRNA genes from culturable and non-culturable mollicutes. J. Microbiol. Methods 14:53-61.

Dermastia, M. 2019. Plant hormones in phytoplasma infected plants. Front. Plant Sci. 10:477.

Efeoğlu, B., Ekmekçi, Y., and Çiçek, N. 2009. Physiological responses of three maize cultivars to drought stress and recovery. S. Afr. J. Bot. 75:34-42.

Foyer, C. H., and Allen, J. F. 2003. Lessons from redox signaling in plants. Antioxid. Redox Signal. 5:3-5.

Gai, Y. P. 2014. Metabolomic analysis reveals the potential metabolites and pathogenesis involved in mulberry yellow dwarf disease. Plant Cell Environ. 37:1474-1490.

Gambino, G., Boccacci, P., Margaria, P., Palmano, S., and Gribaudo, I. 2013. Hydrogen peroxide accumulation and transcriptional changes in grapevines recovered from Flavescence dorée disease. Phytopathology 103: 776-784.

Govindjee, R. 1995. Sixty-three years since Kautsky: Chlorophyll *a* fluorescence. Aust. J. Plant Physiol. 22:131-160.

Heyer, M., Reichelt, M., and Mithöfer, A. 2018. A holistic approach to analyze systemic jasmonate accumulation in individual leaves of Arabidopsis rosettes upon wounding. Front. Plant Sci. 9:1569.

Jiao, D., and Ji, B. 2001. Photoinhibition in *indica* and *japonica* subspecies of rice (*Oryza sativa* L.) and their reciprocal F1 hybrids. Aust. J. Plant Physiol. 28:299-306.

Jones, P., Devonshire, B. J., Holman, T. J., and Ajanga, S. 2004. Napier grass stunt: A new disease associated with a 16SrXI group phytoplasma in Kenya. Plant Pathol. 53:519.

Jung, S., Kim, J. S., Cho, K. Y., Tae, G. S., and Kang, B. G. 2000. Antioxidant responses of cucumber (*Cucumis sativus*) to photoinhibition and oxidative stress induced by norflurazon under high and low PPFDs. Plant Sci. 153:145-154.

Kabirizi, J., Nielsen, S. L., Nicolaisen, M., Byenkya, S., and Alicai, T. 2007. Napier stunt disease in Uganda: Farmers perceptions and impact on fodder production. Afr. Crop Sci. Conf. Proc. 8:895-897.

Kawube, G., Talwana, H., Nicolaisen, M., Alicai, T., Otim, M., Kabirizi, J., Mukwaya, A., and Nielsen, S. L. 2015. Napier grass stunt disease prevalence, incidence, severity and genetic variability of the associated phytoplasma in Uganda. Crop Prot. 75:63-69.

Kehr, J. 2006. Phloem sap proteins: Their identities and potential roles in the interaction between plants and phloem-feeding insects. J. Exp. Bot. 57:767-774.

Koji, S., Fujinuma, S., Midega, C. A. O., Mohamed, H. M., Ishikawa, T., Wilson, M. R., Asche, M., Degelo, S., Adati, T., Pickett, J. A., and Zeyaur, R. 2012. Seasonal abundance of *Maiestas banda* (Hemiptera: Cicadellidae), a vector of phytoplasma, and other leafhoppers and planthoppers (Hemiptera: Delphacidae) associated with Napier grass (*Pennisetum purpureum*) in Kenya. J. Pest Sci. 85:37-46.

Lee, I. M., Davis, R. E., and Gundersen-Rindal, D. E. 2000. Phytoplasma, phytopathogenic mollicutes. Annu. Rev. Microbiol. 54:221-255.

Lee, I. M., Gundersen-Rindal, D., Davis, R., and Bartoszyk, M. 1998. Revised classification of phytoplasmas based on RFLP analyses of 16S rRNA and ribosomal proteins gene sequences. Int. J. Syst. Evol. Microbiol. 48:1153-1169.

León, R., Santamaría, J. M., Alpizar, L., Escamilla, J. A., and Oropeza, C. 1996. Physiological and biochemical changes in shoots of coconut palms affected by lethal yellowing. New Phytol. 134:227-234.

Lepka, P., Stitt, M., Moll, E., and Seemüller, E. 1999. Effect of phytoplasmal infection on concentration and translocation of carbohydrates and amino acids in periwinkle and tobacco. Mol. Plant Pathol. 55:59-68.

Lichtenthaler, H. K. 1987. Chlorophylls and carotenoids: pigments of photosynthetic biomembranes. Methods Enzymol. 148:350-382.

Liu, Z., Zhao, J., and Liu, M. 2016. Photosynthetic responses to phytoplasma infection in Chinese jujube. Plant Physiol. Biochem. 105:12-20.

Mardi, M., Farsad, K. L., Gharechahi, J., and Salekdeh, G. H. 2015. In-depth transcriptome sequencing of Mexican lime trees infected with '*Candidatus* Phytoplasma aurantifolia'. PLoS One 10:e0130425.

Murchie, E. H., and Lawson, T. 2013. Chlorophyll fluorescence analysis: A guide to good practice and understanding some new applications. J. Exp. Bot. 64:3983-3998.

Musetti, R., Buxa, S. V., De Marco, F., Loschi, A., Polizzotto, R., Kogel, K. H., and van Bel, A. J. 2013. Phytoplasma-triggered Ca^{2+} influx is involved in sieve tube blockage. Mol. Plant-Microbe Interact. 26:379-386.

Musetti, R., di Toppi, L. S., Martini, M., Ferrini, F., Loschi, A., Favali, M. A., and Osler, R. 2005. Hydrogen peroxide localization and antioxidant status in the recovery of apricot plants from European Stone Fruit Yellows. Eur. J. Plant Pathol. 112:53-61.

Musetti, R., Marabottini, R., Badiani, M., Martini, M., Sanità di Toppi, L., Borselli, S., Borgo, M., and Osler, R. 2007. On the role of H_2O_2 in the recovery of grapevine (*Vitis vinifera*, cv. Prosecco) from Flavescence dorée disease. Funct. Plant Biol. 34:750-758.

Musetti, R., Pagliari, L., Buxa, S. V., Degola, F., De Marco, F., Loschi, A., Kogel, K. H., and van Bel, A. J. 2016. Phytoplasmas dictate changes in sieve-element ultrastructure to accommodate their requirements for nutrition, multiplication and translocation. Plant Signal. Behav. 11:e1138191.

Nielsen, S. L., Ebong, C., Kabirizi, J., and Nicolaisen, M. 2007. First report of a 16SrXI group phytoplasma "*Candidatus* Phytoplasma oryzae" associated with Napier grass stunt disease in Uganda. Plant Pathol. 56:1039.

Obura, E., Masiga, D., Wachira, F., Gurja, B., and Khan, Z. R. 2011. Detection of phytoplasma by loop-mediated isothermal amplification of DNA (LAMP). J. Microbiol. Methods 84:312-316.

Obura, E., Midega, C. A. O., Masiga, D., Pickett, J. A., Hassan, M., Koji, S., and Khan, Z. R. 2009. *Recilia banda* Kramer (Hemiptera: Cicadellidae), a vector of Napier stunt phytoplasma in Kenya. Naturwissenschaften 96: 1169-1176.

Obura, E. O. 2012. The pathosystem of Napier stunting disease in western Kenya. Ph.D. thesis, Egerton University, Egerton, Kenya.
Oxborough, K., and Baker, N. R. 1997. Resolving chlorophyll *a* fluorescence images of photosynthetic efficiency into photochemical and non-photochemical components—calculation of qP and F_v/F_m; without measuring F_o. Photosynth. Res. 54:135-142.
Paolacci, A. R., Catarcione, G., Ederli, L., Zadra, C., Pasqualini, S., Badiani, M., Musetti, R., Santi, S., and Ciaffi, M. 2017. Jasmonate-mediated defence responses, unlike salicylate-mediated responses, are involved in the recovery of grapevine from bois noir disease. BMC Plant Biol. 17:118.
Paulmann, M. K., Kunert, G., Zimmermann, M. R., Theis, N., Ludwig, A., Meichsner, D., Oelmüller, R., Gershenzon, J., Habekuss, A., Ordon, F., Furch, A. C. U., and Will, T. 2018. *Barley yellow dwarf virus* infection leads to higher chemical defense signals and lower electrophysiological reactions in susceptible compared to tolerant barley genotypes. Front. Plant Sci. 9:145.
Sánchez-Rojo, S., López-Delgado, H. A., Mora-Herrera, M., Almeyda-León, I. H., Zavaleta-Mancera, H. A., and Espinosa-Victoria, D. 2010. Salicylic acid protects potato plants-from phytoplasma-associated stress and improves tuber photosynthate assimilation. Am. J. Potato Res. 88:175-183.
Smirnoff, N., and Wheeler, G. L. 2000. Ascorbic acid in plants: Biosynthesis and function. Crit. Rev. Biochem. Mol. Biol. 35:291-314.
Sugio, A., Maclean, A. M., Kingdom, H. N., Grieve, V. M., Manimekalai, R., and Hogenhout, S. A. 2011. Diverse targets of phytoplasma effectors: from plant development to defense against insects. Annu. Rev. Phytopathol. 49: 175-195.
Tan, P. Y., and Whitlow, T. 2001. Physiological responses of *Catharanthus roseus* (periwinkle) to ash yellows phytoplasmal infection. New Phytol. 150:757-769.
Wamalwa, N. I. E., Midega, C. A. O., Ajanga, S., Omukunda, N. E., Muyekho, F. N., Asudi, G. O., Mulaa, M., and Khan, Z. R. 2017. Screening Napier grass accessions for resistance to Napier grass stunt disease using the loop-mediated isothermal amplification of DNA (LAMP). Crop Prot. 98:61-69.
Wambua, L., Schneider, B., Okwaro, A., Odhiambo, J. W., Imali, O., Nduku, P. W., Agutu, L., Olds, C., Jones, C. S., Masiga, D., Midega, C., Khan, Z., Jores, J., and Fischer, A. 2017. Development of field-applicable tests for rapid and sensitive detection of *Candidatus* Phytoplasma oryzae. Mol. Cell. Probes 35:44-56.
Will, T., and van Bel, A. J. E. 2006. Physical and chemical interactions between aphids and plants. J. Exp. Bot. 57:729-737.
Zafari, S., Niknam, V., Musetti, R., and Noorbakhsh, S. N. 2012. Effect of phytoplasma infection on metabolite content and antioxidant enzyme activity in lime (*Citrus aurantifolia*). Acta Physiol. Plant. 34:561-568.
Zimmermann, M. R., Schneider, B., Mithöfer, A., Reichelt, M., Seemüller, E., and Furch, C. U. 2015. Implications of '*Candidatus* Phytoplasma mali' infection on phloem function of apple trees. J. Endocytobiosis Cell Res. 26: 67-75.